

Live cell lithography: Using optical tweezers to create synthetic tissue†

Utkur Mirsaidov,^a Jan Scrimgeour,^a Winston Timp,^b Kaethe Beck,^a Mustafa Mir,^a Paul Matsudaira^b and Gregory Timp^{*a}

Received 12th May 2008, Accepted 19th August 2008

First published as an Advance Article on the web 1st October 2008

DOI: 10.1039/b807987k

We demonstrate a new method for creating synthetic tissue that has the potential to capture the three-dimensional (3D) complexity of a multi-cellular organism with submicron precision. Using multiple laminar fluid flows in a microfluidic network, we convey cells to an assembly area where multiple, time-shared optical tweezers are used to organize them into a complex array. The cells are then encapsulated in a 30 μm \times 30 μm \times 45 μm volume of photopolymerizable hydrogel that mimicks an extra-cellular matrix. To extend the size, shape and constituency of the array without loss of viability, we then step to an adjacent location while maintaining registration with the reference array, and repeat the process. Using this step-and-repeat method, we formed a heterogeneous array of *E. coli* genetically engineered with a *lac* switch that is functionally linked to fluorescence reporters. We then induced the array using ligands through a microfluidic network and followed the space-time development of the fluorescence to evaluate viability and metabolic activity.

Introduction

Living tissue integrates three essential components—living cells, an extra-cellular matrix (ECM), and external signals—into a complex array that dictates its function. The complexity of the *in vivo* environment is defined, in part, by the social context that develops from the tissue architecture: *i.e.* the distribution of the various cell-types within the scaffold. Synthetic tissue strives to emulate the complexity of the *in vivo* environment to elicit tissue-specific features by controlling, among other things, the positions of the cells and the cell-type on a scaffold that resembles the ECM. There are a number of ways for controlling the cell positions and co-culturing two (or more) cell types on a scaffold including microelectromechanics,¹ soft lithography,^{2,3} optical tweezers,^{4,5} microwells,^{6,7} elastomeric stencils,⁸ electrophoresis,⁹ and dielectrophoresis,¹⁰ and each have advantages and limitations. All of these cell patterning techniques impose restrictions on the substrate such as a special surface chemistry, or electrodes, or optical transparency, *etc.* And none of these techniques have shown the ability to assemble individual cells into precise, repeatable, heterotypic configurations.

We have developed a strategy for creating synthetic tissue that promises to capture the three-dimensional (3D) complexity of a multi-cellular organism with submicron precision. To create synthetic tissue, we exploit laminar fluid flow in a microfluidic network^{11,12} to convey cells to an assembly area where multiple, time-shared optical tweezers¹³ are used to organize them into a complex network. The assembled array is then encapsulated in a photopolymerizable hydrogel, a synthetic scaffold with

a nanostructure that mimics an ECM.¹⁴ Prior work indicates that prolonged exposure to the laser used to form the optical traps damages cells and adversely affects viability.^{15,16} We assessed the potential photodamage in *E. coli* using fluorescent proteins to report on the cell's gene expression and metabolic activity after optical assembly and encapsulation in the synthetic scaffold. We established that under optimum trapping conditions the maximum radiation dose for 50% viability limits the exposure of cell to about 12 min, restricting the assembly time and limiting the maximum size of a single array. However, we show that is possible to extend indefinitely the size and shape of an array using a step-and-repeat methodology in which smaller microarrays of cells are assembled using optical tweezers in less than 12 min, fixed in individual, well-defined hydrogel microstructures, and then tiled together into a significantly larger, well registered, super-array.

As a demonstration, we have created synthetic biofilms made from multiple strains of bacteria. A biofilm shows many essential aspects of tissue. It is a sessile community comprised of phenotypes differentiated from planktonic bacteria in response to environmental cues and quorum-sensing signals, all encapsulated in a hydrated matrix of polysaccharides, proteins and exopolymeric substances—it is like a city of microorganisms.¹⁷ The genetically engineered bacterial strains that we use to produce a synthetic biofilm represent an especially stringent test of our method for creating tissue because they are so small (2 μm \times 0.5 μm) and because, aside from their distinct reporter plasmids, the phenotypes are practically indistinguishable.

Results and discussion

Array assembly

Tissue is comprised of different cell types, but without clear morphological differences, sorting, organizing and assembling the different types into tissue using just optical tweezers can be problematic. So, to avoid mixing them, we convey *E. coli*

^aBeckman Institute, University of Illinois at Urbana-Champaign, 405 North Mathews Avenue, Urbana, IL, 61801, USA. E-mail: gtimp@uiuc.edu; Fax: +1 217-244-6622; Tel: +1 217-244-9629

^bWhitehead Institute, Massachusetts Institute of Technology, Cambridge, MA, 02319, USA

† Electronic supplementary information (ESI) available: Hydrogel optimization (Fig. S1 and S2). See DOI: 10.1039/b807987k

carrying one of three plasmids coded G1, R1, and Y1 to an assembly area using multiple laminar fluid flows in a microfluidic device (like that represented schematically in Fig. 1(a)). The plasmids allow either EGFP (enhanced green fluorescent

protein), mRFP1 (red fluorescent protein) or YFP (yellow fluorescent protein) to be produced under control of the *lac* switch. In naïve cells, the *lac* repressor protein (*lacI*) binds to the promoter region of the *lac* operon, preventing transcription, but in the presence of an inducer such as isopropyl β -D-thiogalactopyranoside (IPTG) the repressor structure is altered by the inducer, preventing binding to the DNA and allowing expression of the fluorescent protein. Based on increasing cellular fluorescence, we can infer the activity of the cell's metabolism after the induction of gene expression. Fig. 1(b) is a micrograph of the fluorescence observed in the microfluidic network using multiple flows moving at a rate of $10 \mu\text{L min}^{-1}$, carrying R1 cells on the right and G1 on the left, that have been induced with IPTG. Notice that the G1 and R1 strains do not mix in the microfluidic due to the laminar flow: *i.e.* the center channel remains free of bacteria. Accordingly, it is practical to assemble and organize the cells, capturing bacteria either one-at-a-time or *en masse* from one or the other of the outer flows according to the desired specifications of the array.

Using tweezers formed from the optics represented schematically in Fig. 1(a), we assembled heterotypic arrays of bacteria in the central channel of the microfluidic as illustrated by the microarray in the inset. The tweezers are formed from a continuous wave (CW) Ti:Sapphire laser beam using a combination of two different diffractive elements, acousto-optic deflectors (AODs) and a spatial light modulator (SLM), to produce time-shared holographic optical traps (HOTs). The position of each trap can be controlled with $\pm 18 \text{ nm}$ precision. The heterotypic two-dimensional (2D) 5×6 microarray shown in the inset was assembled from G1 and R1 strains using a time-averaged optical power of $\sim 4 \text{ mW}$ per trap at a wavelength of $\lambda = 900 \text{ nm}$. The multi-channel fluorescence image demonstrates the capability to sort and assemble different cell types.

While optical trapping can be used to create vast networks of cells resembling tissue, the trapping beam must still be held on the cells to maintain the array. To minimize exposure to the laser beam, we fixed the position of the cells semi-permanently^{18,19} in a bio-compatible scaffold made from a photopolymerizable poly (ethylene glycol) diacrylate (PEGDA) hydrogel. PEGDA hydrogels are especially attractive for use as synthetic scaffolds because the photopolymerization time can be relatively short ($\sim 1\text{--}3 \text{ s}$)¹⁰ and it is porous,²⁰ allowing for transport of nutrients to the cell and removal of waste.²¹ Hydrogels have been shown to maintain viability and activity of bioluminescent *E. coli* for up to two weeks without a change in the dose-dependent induction.²²

Once an array like that shown in the inset to Fig. 1(a) is assembled with optical tweezers, the pre-polymer solution in the clear channel is exposed to UV light to form a gel as shown in Fig. 1(c). Fig. 1(c) shows a volume reconstruction of a $2\text{D } 4 \times 4$ array of the G1 *E. coli* assembled using a time-averaged power of $\sim 4 \text{ mW}$ per trap at $\lambda = 900 \text{ nm}$ and then encapsulated in an optimized hydrogel spot. After encapsulation, the array and hydrogel were stained with SYTO9 and rhodamine B respectively and imaged using a laser scanning confocal microscope (Leica). To achieve a hydrogel microstructure suitable for tiling we explored the effects of the photo-initiator concentration; PEGDA concentration; the UV power; wavelength; and exposure on hydrogel size, array definition, and bacterial viability (see ESI[†]). Based on this analysis, we chose to use a pre-polymer

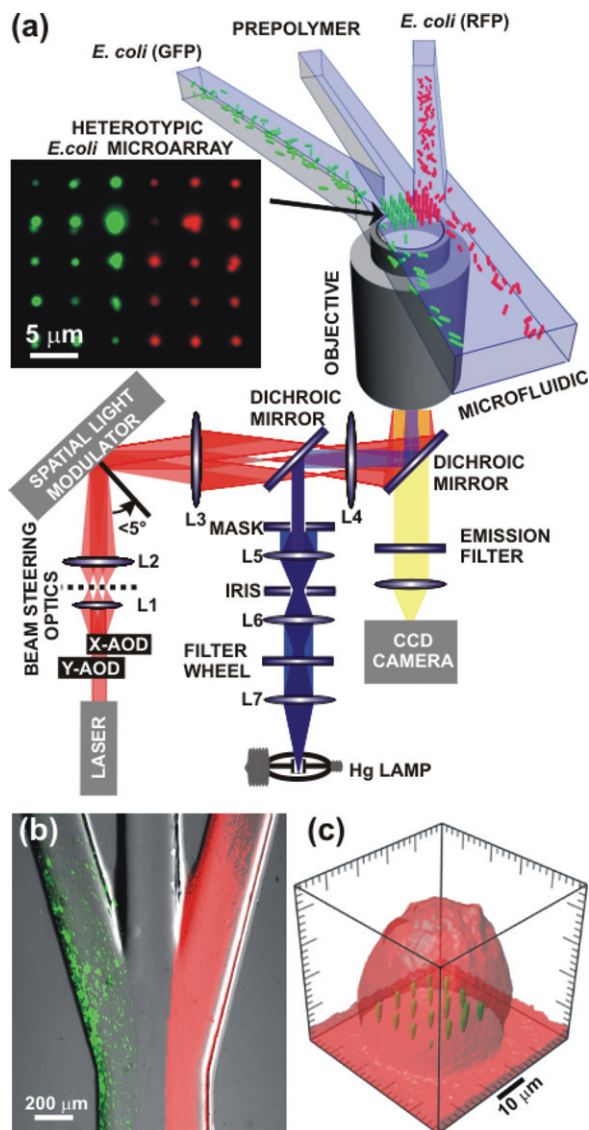


Fig. 1 Schematic diagram of a time-shared holographic optical trapping apparatus and microfluidic conveyer. (a) Cells are manipulated using time-multiplexed, 3D arrays of optical traps formed with infrared light (red path) from a Ti:sapphire laser beam steered with two acousto-optic deflectors and a spatial light modulator, and focused with a high N.A. objective in a commercial optical microscope. The same microscope is also used for imaging (yellow path) and UV exposure of the hydrogel (blue path). (Inset) An example of a $2\text{D } 5 \times 6$ heterogeneous microarray of G1 (green fluorescence) and R1 (red fluorescence) *E. coli* strains embedded in hydrogel formed using this apparatus. The fluorescence demonstrates the reliable sorting achieved using the microfluidic network. (b) Cells are conveyed to the assembly area using a microfluidic network: one cell type (red) flows on the right, another (green) flows on the left, while the central channel is cell-free. The flow in the microfluidic shown is $10 \mu\text{L min}^{-1}$. The hydrogel is then formed in the clear channel to avoid contamination. (c) Volume reconstruction obtained from confocal image of the 4×4 microarray encapsulated inside an optimized hydrogel spot.

solution consisting of 3.4 kDa PEGDA dissolved at 8% (w/v) in M9 minimal media with 0.1–0.2% (v/v) photo-initiator (2-hydroxy-2-methyl-propriophenone). Hydrogel microstructure definition was optimized at $\sim 40 \mu\text{W}$ of UV power for exposure times below 1.8 s. This combination affords a wide process window for concentrations in the pre-polymer solution and exposure conditions, accommodating changes in the UV lamp intensity with time, *etc.* Viability in individual microarrays can be as high as 95%–100% with optimal handling by tweezers. But typically, with assembly times of 6–7 min, we expect the viability to approach that of the control population ($\sim 85\%$), which sets the target for viability in larger super-arrays (see Fig. 5 later).

To facilitate precise registration of neighboring arrays, and minimize the distortion that occurs during polymerization, a mask was inserted at the field stop of the Köhler illumination system (*i.e.* between $L4$ and $L5$ in the schematic shown in Fig. 1(a)) to produce a square field of uniform intensity in the focal plane of the objective.²³ The resulting hydrogel microstructures are approximately square in the trapping plane, however, they round quickly as the intensity falls along the optic axis. The typical dimensions of the hydrogel were about $30 \mu\text{m} \times 30 \mu\text{m} \times 45 \mu\text{m}$ (X, Y, Z) as shown in Fig. 1(c). The organization of the array is well preserved during encapsulation, but the mean change between the pre- and post-gelling position of the bacteria was $1.2 \mu\text{m}$. Since it is repeatable (see below) the deformation that occurs could be compensated by pre-positioning the cells appropriately. Shrinking the size of the illuminated area had little effect on the size of the hydrogel microstructure, presumably due to rapid free radical diffusion in the low viscosity pre-polymer. Greater control over the size and definition of the gel can be achieved: by reducing the molecular weight of the PEDGA, increasing its concentration, increasing the photo-initiator concentration, and reducing the oxygen concentration in the prepolymer solution. However, these solutions can compromise the bacterial viability.

3D array

To elicit tissue-specific features, synthetic tissue should mimic not only the heterotypic environment, but also its 3D architecture. Using time-shared HOTs in conjunction with microfluidics, we assembled a 3D, heterogeneous living cell microarray in hydrogel without loss of viability. Fig. 2(a–d) show a 3D $1 \times 3 \times 3$ microarray comprised of two 1×3 rows of Y1 *E. coli* and one row of 1×3 of R1 *E. coli*, each 1×3 array offset by $9 \mu\text{m}$ along the (Z) optic axis and $6 \mu\text{m}$ along the X -axis. The traps were formed with a time-averaged power per trap of $\sim 5 \text{ mW}$ at $\lambda = 900 \text{ nm}$. To form this microarray, the AODs in Fig. 1(a) were used to generate a single, linear 1×3 time-shared array, while a phase-only hologram displayed on the SLM split the time-shared beam into three components with different divergences to create the 3D array,

The 3D nature of the array is indicated by the three distinct focus conditions shown in Fig. 2(a–c) and explicitly shown in a volume reconstruction from confocal data shown in the inset to (d). For example, in Fig. 2(b) the camera focal plane is coplanar with middle 1×3 array of Y1 cells located at $Z = 9 \mu\text{m}$, causing the bottom array ($Z = 0 \mu\text{m}$) to be over-focused and the top array ($Z = 18 \mu\text{m}$) to be slightly under-focused. The limited extent of the array along Z —the maximum range is about $\pm 20 \mu\text{m}$ —is related to the trapping potential associated with the optical tweezers²⁴ and the velocity profile in the microfluidic. To trap in a higher velocity flow at mid-height in the microfluidic requires more optical power, which adversely affects cell viability (see below). The recent development of layer-by-layer microfluidic approaches for creating biomimetic 3D structures suggests that this is not a fundamental limitation for tissue synthesis.^{11,12,25}

After assembly, the cells were encapsulated in hydrogel and then induced (at $t = 0$) to express mRFP1 and YFP by broadcasting 2 mM IPTG using a $0.05 \mu\text{L min}^{-1}$ flow. Subsequently, we followed the development of the fluorescence in each

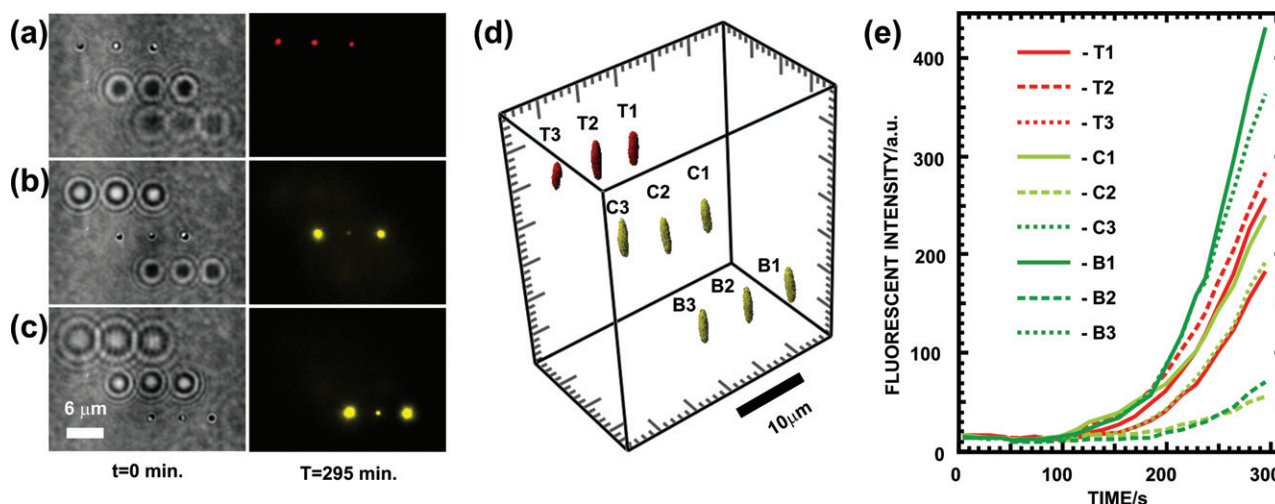


Fig. 2 Gene expression in a heterogeneous 3D $3 \times 1 \times 3$ microarray comprising R1 and Y1 *E. coli*. (a–c) Transmission micrographs with the focus at $Z = 18 \mu\text{m}$, $9 \mu\text{m}$ and $0 \mu\text{m}$, respectively at $t = 0$ just prior to induction with IPTG. Two 1×3 arrays of Y1s are located at $Z = 0 \mu\text{m}$ and $9 \mu\text{m}$, while a 1×3 array of R1s is located at $Z = 18 \mu\text{m}$. IPTG, introduced through the microfluidic, triggers production of mRFP1 (red fluorescence) and YFP (yellow fluorescence). At $t = 295 \text{ min}$ red and yellow fluorescence can be observed as illustrated by the fluorescence micrographs showing the red (top), yellow (middle) and yellow (bottom) channels. (d) Volume reconstruction of the array based confocal data, demonstrating the 3D nature of the array. (e) Time development of the fluorescence for each cell in the array.

individual cell in the array using time-lapse images; the results are summarized in Fig. 2(e). The onset of red and yellow fluorescence was observed at nearly the same time, about 100 min after induction, indicating that mRFP1/YFP is being produced in the cells trapped in the array. As time progressed beyond 100 min, the fluorescent intensity increases monotonically and eventually the cells start to replicate—an unambiguous sign of viability. But as Fig. 2(e) shows, there are differences in gene expression among the individuals in the array, presumably arising from stochastic noise in otherwise identical cells. We attribute the differences to variations in the initial plasmid copy number (~ 15), the individual cell metabolism, and variations in the timing of cell division. Thus, it should be possible to study stochastic effects in a synthetic tissue element comprised of microarrays like this, provided the number and architecture of the cells captures the complexity of actual tissue.

A large array of viable cells with precise positional control is indispensable for studying the relation of individual cells to their community. But to use optical tweezers to create arrays with more elements that capture the complexity of actual tissue, the cells comprising the array would have to suffer extended exposure to the trapping beam to allow for the increased time required for assembly. We have already shown that it is possible to produce arrays with >400 cells,²⁶ but viability is adversely affected by the long duration exposure to the beam (prior to photopolymerization).¹⁵

Fig. 3 summarizes the effect of the duration of exposure to a time-shared optical trap on viability in 2D 5×5 microarrays of G1 *E. coli*. Cells were exposed to a time-averaged power of ~ 4 mW per trap, and held (in the array) for times ranging from 4 to 15 min prior to encapsulation. After rinsing with M9, M9 containing 2 mM IPTG was broadcast into the array at $0.1 \mu\text{L min}^{-1}$ flow. Live cells exhibited green fluorescence within about 100

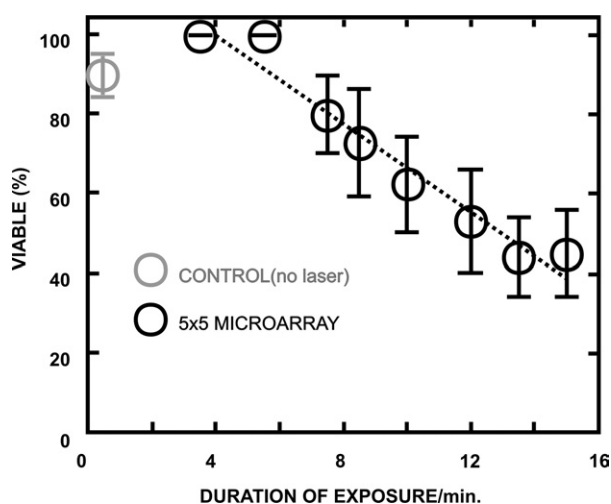


Fig. 3 Exposure to the optical trap beam has a deleterious affect on *E. coli* viability. 2D 5×5 arrays of *E. coli* bacteria incorporating the plasmid G1 were assembled with trapping times, ranging from 4 min to 15 min. (The zero minute datum shown in grey on the plot represents the control with no exposure to the laser.) After induction the development of the fluorescence was followed for 5 h before scoring. The viability degrades linearly with the duration of exposure to the optical trap, with the LD_{50} estimated at 12 min.

min. We scored the fluorescence from each element in the different arrays after 5 h and found that the number of fluorescent cells decreases monotonically with increasing trap duration from 100% viable at 4 min to less than 50% at 15 min. We found a dose of ~ 720 s (12 min) to be lethal for about 50% of the array population (LD_{50}). Thus, photodamage presents a fundamental limitation on the size of the array. This limitation is especially crippling when assembling the array one cell at a time. Larger arrays can be created by filling multiple traps simultaneously, but this often results in capturing multiple cells per trap. Even if the assembly process is automated,¹³ and the cell velocity between the laminar flow and the final location in the array is increased, viability is still likely to be a limitation since the power in the trap has to be increased to compensate for the escape force due to the viscous drag associated with a high velocity flow.

Step-and-repeat

Nevertheless, within the parameters defining the optical trap and the hydrogel scaffold, it is still possible to extend the size, shape and constituency of the array without compromising viability by using a step-and-repeat methodology. Step-and-repeat involves assembling a super-array of living cells out of a composite of microarrays, each consisting of a small number of cells that are assembled and encapsulated in hydrogel in <12 min so that viability is not compromised.

To demonstrate the flexibility of this approach we assembled a super-array of heterogeneous microarrays of *E. coli*. Each microarray is comprised of two regular 2×2 microarrays—one of G1 and another of R1 cells—with elements spaced $4.3 \mu\text{m}$ apart. The microarrays are assembled in <6 min with bacteria captured from the two outer channels in the microfluidic. Adjacent microarrays were spaced $30 \mu\text{m}$ apart (in *X* and/or *Y*), using a motorized X-Y stage (Zeiss DC $4'' \times 4''$) with $0.25 \mu\text{m}$ step resolution. Fig. 4(a) shows a bright field (transmission) image of the array taken at $t = 0$, just prior to induction with IPTG, while Fig. 4(b) shows the corresponding fluorescence observed in the same array 600 min later. The onset of fluorescence was observed about 180 min after induction. After 10 h, we find that 75% of the *E. coli* are still viable and in some cases have replicated.

Fig. 4(c) depicts the registration between neighboring microarrays. The positions of the individual bacteria were determined from brightfield images using a MATLAB particle tracking routine.²⁷ The deviation in the bacterial positions was measured relative to the reference array. The mean displacement from the expected positions was 300 nm , with a maximum displacement of $\sim 900 \text{ nm}$, demonstrating that the tiling strategy is capable of submicron resolution in a cell position. The repeatability of the displacements between arrays indicates that the deformation within an array is repeatable. Thus, the deformation that occurs while gelling does not represent a limitation on registration precision—it is possible to compensate for it by pre-positioning the cells in the array.

This is the largest heterogeneous cell array ever synthesized with such precision. And this same strategy can readily be generalized to different architectures with multiple cell types and 3D without compromising viability or precision. Moreover, arrays formed by step-and-repeat are highly reproducible and allow for *in situ* single-cell analysis in a user-defined

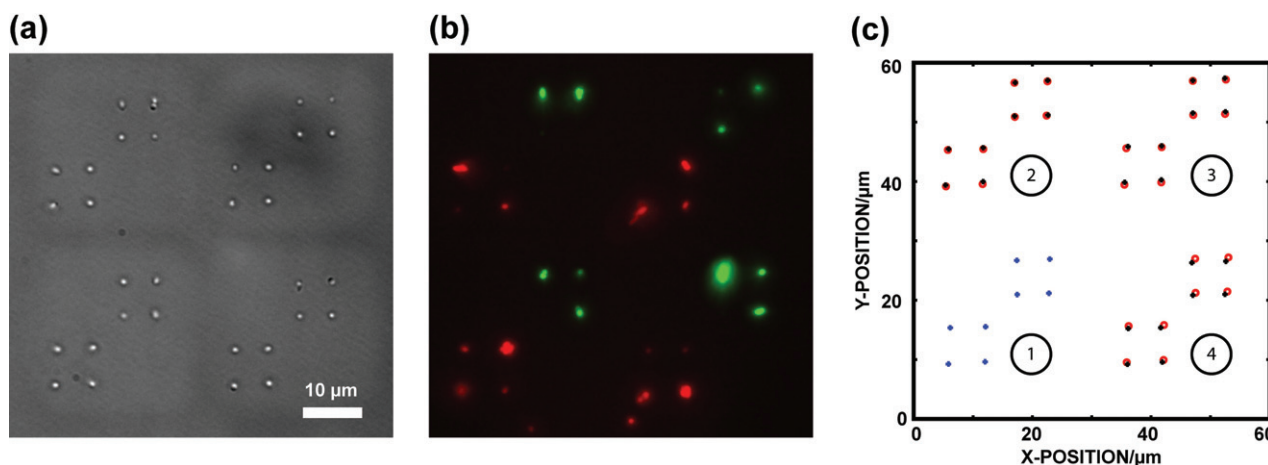


Fig. 4 2×2 microarrays of G1 and R1 *E. coli* form a high precision, heterogeneous, 2×2 super-array. G1 and R1 *E. coli* were assembled in the same microarray. Adjacent hydrogel spots are separated by $30 \mu\text{m}$. (a) Bright-field image taken at $t = 0$ just prior to the broadcast of 2 mM IPTG to the super-array using the microfluidic, and (b) Multi-channel fluorescent image of the same array taken 600 min later showing the development of GFP and RFP fluorescence. All images were taken with a $100\times$ objective with 1.3 N.A. 75% of the cells remain viable after 5 h as scored by the fluorescence. (c) Particle tracking analysis of the bacterial array shows that the bacteria are aligned with submicron precision, + (blue) first (reference) encapsulated array, + (black) subsequent arrays and O (red) projected positions of the second, third and fourth array. The numbers in the bottom right of each microarray denote the assembly order.

microenvironment. In contrast, flow cytometry, which is currently the standard method for single-cell fluorescent analysis of large populations, cannot be used to measure the behavior of individual cells *in a social context* over time. Flow cytometry is a destructive measurement technique, requiring multiple samples to be harvested to assemble a time-series, making it difficult to examine how individual cells respond over time. Synthetic tissue formed by step-and-repeat provides a platform for the long term observation of individual cells in the social context of a large array while maintaining control over their microenvironment.

Fig. 5 shows two super-arrays assembled using the same step-and-repeat methodology. Both super-arrays were assembled from homogenous 4×4 microarrays containing G1 *E. coli*. Fig. 5(a,i) and (b,i) show transmission images of the super-arrays taken at $t = 0$, just prior to IPTG induction *via* the microfluidic; Fig. 5(a,ii) and (b,ii) show the corresponding fluorescence images of the same super-arrays taken 220 min and 270 min after induction, respectively. Fig. 5(a,iii) and (b,iii) show volume reconstructions of each array. Scoring by the observed fluorescence, about 70% of the cells remain viable after 5 h in Fig. 5(a,ii). The viability in the bottom row is noticeably reduced though and these microarrays were the first to be assembled. We tentatively attribute the diminished viability in this row to repeated exposure to free radicals formed during photopolymerization. This hypothesis is supported by a trend showing 51% viability in a larger 4×4 super-array of 4×4 microarrays containing G1 *E. coli* that is described in the supplement.

To test this hypothesis, we formed a 3×4 super-array of homogenous 4×4 microarrays, containing G1 *E. coli*, with staggered rows and increased centre-to-centre spacing in each row to $60 \mu\text{m}$ to promote convective flow between microarrays. The gap between the microarrays is evident in the transmission micrograph shown in Fig. 5(b,i). The dominant transport mechanism in the vicinity of the hydrogel is diffusion for low flow (with Péclet number < 1), while convection dominates beyond the gel boundary. Fig. 5(b,ii) shows the fluorescence from the super-array

270 min after induction. We find that 83% of the cells remain viable, which is comparable to the control population (85%). Presumably, free radicals generated by photopolymerization are more effectively removed from each microarray in this geometry, limiting the exposure of the surrounding microarrays.

Experimental

Genetically engineered bacteria

DH5 α bacteria (Invitrogen) were transformed with one of three plasmids, G1, Y1 or R1. G1 carries an ampicillin resistance and a medium copy (20–30 copies per cell) origin of replication (pBR322). It has eGFP under the control of the *lac* operon. Y1 and R1 both carry a kanamycin resistance gene and a medium copy (15–25 copies per cell) origin of replication (p15a). They have YFP and mRFP1, respectively, under the control of the *lac* operon.

The transformed bacteria were grown in M9 (0.2% glycerol) minimal media supplemented with $200 \mu\text{M}$ thiamine and 0.2% (w/v) casamino acids with either ampicillin ($100 \mu\text{g mL}^{-1}$) or kanamycin ($100 \mu\text{g mL}^{-1}$) as a selection marker. They were grown overnight at 37°C , diluted 1 : 10 into fresh media, regrown at room temperature, and harvested when they reached an optical density (OD_{633}) of 0.6–0.7. The bacteria were then centrifuged twice at 800 g for 2 min. Between each spin cycle the supernatant was aspirated, and the bacterial pellet re-suspended in M9 media. After the final wash the bacteria were re-suspended in M9 (7% glycerol) containing the photo-initiator, 2-hydroxy-2-methyl-propionone, at a concentration of 0.2% (v/v). Subsequently, the cell suspensions were loaded into individual 1 mL syringes. The excess glycerol in the media was used to balance the viscosity and density of the fluids in each channel of the microfluidics.

Pre-polymer solution

Hydrogel pre-polymer solution consisted of PEGDA (MW = 3400 Da) (Laysan Bio) dissolved in M9 (0.2% glycerol) minimal

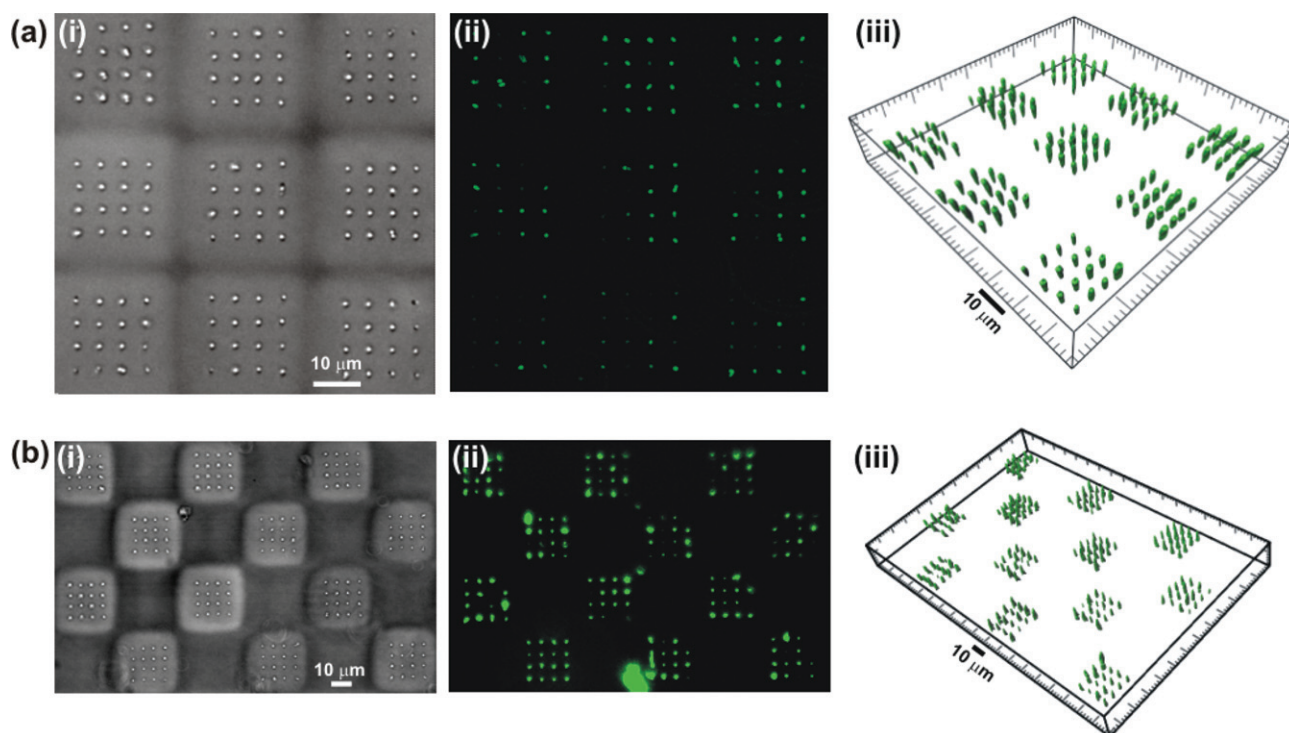


Fig. 5 Two super-arrays of G1 *E. coli*. (a) Nine homogeneous 4×4 microarrays of G1 *E. coli* forming a 3×3 super-array. (a,i) Transmission image of the super-array at $t = 0$, when IPTG is broadcast into the array *via* the micro fluidic. (a,ii) Fluorescence image of the same super-array 220 min later. The images were taken a $40\times$ objective with 0.95 N.A. 70% of the cells remain viable after 5 h. The viability of the bottom row in the 3×3 super-array, which was assembled first, seems especially problematic. (a,iii) Volume reconstruction of the same super-array obtained from confocal images. (b) Twelve homogeneous 4×4 microarrays of G1 *E. coli* form a 3×4 super-array with staggered spacing. (b,i) Transmission image of the super-array at $t = 0$, when IPTG is broadcast into the array *via* the microfluidic. (b,ii) Fluorescence image of the same super-array 270 min later. About 83% of the cells remain viable after 5 h. We attribute the improvement in viability relative to the super-array of part (a) to flow around the microarrays and a concomitant reduction in exposure to free radicals formed during photopolymerization. (b,iii) Volume reconstruction of the same array obtained from confocal images. The images were taken using a 50 ms exposure through a $40\times$ objective with 0.95NA.

media to yield 8% (w/v) final concentration and the photo-initiator, 2-hydroxy-2-methyl-propiophenone (Sigma), at a concentration of 0.1–0.2% (v/v). The pre-polymer mixture was vortexed for 1 min, and then loaded into 1 mL syringes. All the syringes carry the photo-initiator to avoid creating a concentration gradient that could affect the exposure conditions required for polymerization of the hydrogel in the microfluidics. The cells were not suspended directly in the pre-polymer to avoid the rapid aggregation of bacteria that occurs in PEGDA. Before loading with cells and pre-polymer, the microfluidic channels were pre-loaded with degassed M9. Tubing was attached to each syringe *via* a 23 gauge needle; it was then filled and the connected to the microfluidics. Bubble merging between the tubing and the device ensured that no bubbles were introduced to the system. The syringes were placed in a syringe pump (Harvard Apparatus) and the system was flushed for 5 min at $20 \mu\text{L min}^{-1}$, to remove stray cells produced during the loading process. To stabilize the system at a suitable flow velocity for optical trapping the flow rate was slowly reduced to $0.05 \mu\text{L min}^{-1}$ over 2 min.

Microfluidics

We used multiple laminar fluid flows in a microfluidic device to convey cells to an assembly area as illustrated in Fig. 1(a). The microfluidic device consisted of a three channel Y-junction

similar to that shown in Fig. 1(b). The three entry-channels, which are $200 \mu\text{m}$ wide, merged with an angle of 15° between neighboring channels into a single $600 \mu\text{m}$ wide exit-channel. All the channels were $200 \mu\text{m}$ in height. The microfluidic device was formed from poly (dimethylsiloxane) (PDMS) using a mold-casting technique. A master mold, generated using stereolithography (FineLine Prototyping), is made of a DSM Somos ProtoTherm 12120, a strong, high temperature tolerant plastic. To detach the PDMS without tearing the device, the mold is coated with a fluoropolymer, (Tridecafluor-1,1,2,2, Tetrahydrooctyl)-1-Trichlorosilane, using vapor deposition at 75°C and house ($20''$ Hg) vacuum for 2 h.²⁸ The PDMS, Sylgard 184 (Corning), base and curing agent are mixed (by volume) in the ratio 5 : 1, to increase the mechanical rigidity of the device, and degassed at house vacuum for 30 min. This mixture was poured into the master mold, and then cured at 75°C for ~ 2 h. After cooling, the PDMS was peeled away from the mold, yielding a piece of silicone with the inverse replica of the master mold. Holes are punched in the silicone chip at the input and output ports using a blunt syringe needle to allow tubing to be attached. This device is completed by attaching the PDMS to a cover glass (#1) using oxygen plasma; giving a system that is suitable for both high-resolution imaging and optical trapping.

To enhance hydrogel adhesion, and prevent bacterial adhesion, the internal surfaces of the microfluidic device are treated

with a methacrylate silane, which will crosslink with the hydrogel.^{29,30} Acrylate coatings have also been shown to prevent bacterial adhesion in previous work.³¹ A 2% (v/v) solution of 3-(trimethoxysilyl) propyl methacrylate (Sigma) was made in 10 mL of 95% ethanol. The solution was adjusted to pH 5 using 50 μ L of glacial acetic acid. 500 μ L of this solution was pushed through the microfluidic chip using a 1 mL syringe, and incubated for 5 min at room temperature. The chip is then flushed with 5 mL of deionized water and placed in an oven overnight at 75 °C. Finally, the chip is flushed with argon for 2–3 h at 5 psi, to remove oxygen that inhibits free-radical polymerization.

Optical tweezers

Optical traps were formed, at a wavelength $\lambda = 900$ nm using a tunable CW Ti:Sapphire laser (Spectra Physics) pumped at 532 nm by a 10 W Nd:YVO₄ diode-pumped solid state laser (Spectra Physics). Acousto-optic deflectors (AA-Optoelectronic), were used to form time-shared optical traps from the single CW Ti:Sapphire beam. Two orthogonally mounted AODs give independent control of the x - and y -position of a trap, allowing the formation of 2D microarrays of optical traps. All the microarrays were generated with a dwell time of 10 μ sec at each position. The time-shared beam can be further manipulated to yield 3D optical traps using a SLM (Boulder Nonlinear Systems). This electrically addressed nematic liquid crystal device acts as a 256 level kinoform in the optical path. 512 by 512 pixel kinoforms were calculated using the Gerchberg-Saxton algorithm.³²

The diffractive optical elements (AODs and SLM) are placed in planes conjugate to the back aperture of the microscope objective using relay lenses. The afocal optical system comprises lenses L1 ($f = 20$ cm), L2 ($f = 40$ cm), L3 ($f = 40$ cm), L4 ($f = 40$ cm). The focal lengths of lenses L1, L2, L3, and L4, and the separation between them are chosen to ensure that deflections of the beam produce only a change in the angle of the beam entering the back aperture of the microscope objective. Typically, the cells were trapped about 5 μ m above the surface of the cover glass to minimize spherical aberrations from the media. The laser power was measured at the back aperture of the trapping objective, 1.3 N.A. 100 \times FLUAR (Zeiss) and corrected for the transmission through the objective using transmission curves provided by Zeiss.³³ The transmission at $\lambda = 900$ nm was approximately 68%. Laser powers are quoted as time-averaged powers based on the duty cycle (*i.e.* the number of traps) in the time-shared array.

EPI-fluorescence

An EXFO[®] metal halide light source is used for fluorescence imaging and to generate the UV light needed to photo-polymerize the hydrogel. The light generated by the lamp is focused using a Köhler light train, as shown in Fig. 1, lenses L4 ($f = 40$ cm), L5 ($f = 25$ cm), L6 ($f = 30$ cm) and L7 (Exfo collimator: 810–00022). A dichroic mirror (Chroma) combines the UV/visible epifluorescence train and the near infrared optical tweezers. A filter wheel (Ludl) allows wavelength selection, and precise control of exposure times. The power reaching the objective was controlled by an iris contained within the EXFO[®] source.

Fluorescent proteins GFP/mRFP1 were imaged using filter sets 59022 GFP/mCherry (CHROMA), while YFP/mRFP1 was

imaged using filter set 69308 CFP/YFP/mCherry (Chroma). Single band excitation filters were used in all cases and images were captured on a cooled CCD camera (Hamamatsu). The photo-initiator was excited using a 340 ± 13 nm UV filter (Semrock) which maximizes the efficiency of free radical generation while minimizing the overall UV exposure. To control the shape of the UV illumination field and the resulting gel spot, a square mask ($\sim 5.6 \times 5.6$ mm) is placed in the field stop of the Köhler train. This resulted in a uniformly illuminated 23×23 μ m square in specimen plane. UV power reported in Fig. S1(a–b)[†] was measured at back focal plane of the objective. UV exposure and time-lapse imaging was controlled by code written in LabVIEW (National Instruments). The transmission of the Zeiss Fluor 100 \times objective used for this work at 340 nm is approximately 75%.

Multi-channel assembly

Heterotypic microarrays of bacteria were assembled using a time-averaged power of ~ 7.5 mW per trap. All the trapping took place in the immediate vicinity of the junction in the microfluidic between the central and outer channels (flow rate of 0.05 μ L min^{-1}). Bacteria were captured individually and placed into the time-shared array of optical traps using a freely definable shepherd beam; time-averaged powers in the array and shepherd beam were 7.5 mW and 22.5 mW respectively. Cells were exposed to the shepherd beam for no more than 10 s. Assembly of the 2×2 heterogeneous microarrays required ~ 6 min per microarray: 1 min is used to organize one of the bacterial strains constituting the microarray; 2–3 min are required to traverse the central channel; another minute to trap and organize the second strain in the microarray; and finally 1 min is used to reach the final array site. Completed heterotypic microarrays were pulled back into the central leg of the microfluidic and fixed in a square hydrogel microstructure using a 1.5 s duration exposure of UV (38 μ W at 340 ± 13 nm). The microfluidic was reset by flushing at a rate of 20 μ L min^{-1} for 1 min; the flow rate was reduced to 0.05 μ L min^{-1} ; and the process was repeated. Once the super-array was complete the microfluidic was flushed through the central channel with 5 mL of M9. M9 containing 2 mM IPTG (flow rate 0.2 μ L min^{-1}) was then used to trigger expression of fluorescent protein in the bacteria. Fluorescence images of protein expression were captured every 15 min for 12 h.

Homogeneous arrays were assembled in a similar manner with the outer channels containing the same cell type. Bacteria from both outer channels were used to assemble the super-array and minimize the distance bacteria had to be translated to the assembly area.

Confocal microscopy and image processing

Confocal microscopy was performed on a Leica SP2 (Leica Microsystems). All confocal images were acquired using a 1.4 N.A. 63 \times oil immersion objective. Confocal image stacks were processed in Imaris (Bitplane). Conventional fluorescence images were processed using ImageJ (NIH), MATLAB (Mathworks) and Imaris.

Conclusion

We have established that optical tweezers can be used in conjunction with a microfluidic to sort and synthesize

heterogeneous 3D microarrays of *E. coli* in hydrogel, but photodamage due to the tweezers restricts the size of the microarrays, especially if the cells are loaded one at a time. The LD₅₀ for a ~4 mW time-averaged laser beam at $\lambda = 900$ nm is about 720 s. Using a step-and-repeat method, viable microarrays assembled in <720 s can form the basis for much larger arrays—super-arrays—but viability in the super-array appears to be compromised by repeated exposure of the cells to the free radicals used to polymerize the hydrogel. However, by staggering the microarrays within the super-array, diffusion of the radicals between microarrays and the concomitant damage can be avoided. Using this strategy, we have synthesized super-arrays comprised of ~200 cells with submicron registration in *X*, *Y* and *Z* without compromising viability measured relative to the control population. Bacteria will escape from an optical trap with a time-averaged power (<7.5mW per trap) if the translation velocity in the pre-polymer solution exceeds 80–100 $\mu\text{m min}^{-1}$ because of the viscous drag exerted by the liquid. Consequently, the maximum area of the super-array is limited by the duration of exposure at this velocity to about $350 \times 350 \mu\text{m}^2$.

Synthetic tissue this size could provide a platform for the development of more complex *in vitro* assays. Such a platform affords control of the cellular microenvironment and at the same time allows for the examination of cells in a well defined social context with single cell resolution to gain a deeper understanding of cellular behavior in tissue. We demonstrated that it is possible to create a synthetic biofilm. Assembling a synthetic structure that resembles a real-world bacterial biofilm could be the key to tuning the behavior of bacteria or discovering an antibiotic for inhibiting infection—biofilms are involved in 60% of all infections.³⁴ Currently, a popular method for studying biofilms is based on passing a bacterial suspension through a flow-cell to which cells adhere and grow into a biofilm.³⁴ A flow cell offers no control of the architecture—only single species biofilms have been studied so far. Moreover, the inability to assess the chemical gradients or gradients of gene expression in a biofilm presents another challenge to current research. Almost every study to date uses DNA microarray or proteomic analysis of a biofilm population to take an *average* of the expression profile of the entire population ignoring gradients. In contrast, using optical tweezers in conjunction with a step-and-repeat method to create a synthetic biofilm in a microfluidic provides control over the architecture of the film (or any tissue), while still affording some exogenous control of the microenvironment of the cell and the chemical gradients in the film through the microfluidic device. Thus, this new tool fills a niche in the continuum between the complex and highly variable data provided by real-world models and tissue samples and the reductionist *in vitro* cellular assay data.

Acknowledgements

We gratefully acknowledge iGEM for help with plasmid construction. This effort is partially supported by an NSF NIRT # 0404030 and a Beckman Foundation Grant.

References

- 1 E. E. Hui and S. N. Bhatia, *Proc. Natl. Acad. Sci. U. S. A.*, 2007, **104**, 5722.
- 2 C. S. Chen, M. Mrksich, S. Huang, G. M. Whitesides and D. E. Ingber, *Science*, 1997, **276**, 1425–1428.
- 3 R. Singhvi, A. Kumar, G. P. Lopez, G. N. Stephanopoulos, D. I. Wang, G. M. Whitesides and D. E. Ingber, *Science*, 1994, **264**, 696–698.
- 4 J. Enger, M. Goksör, K. Ramser, P. Hagberg and D. Hanstorp, *Lab Chip*, 2004, **4**, 196–200.
- 5 E. Eriksson, J. Enger, B. Nordlander, N. Erjavec, K. Ramser, M. Goksör, S. Hohmann, T. Nyström and D. Hanstorp, *Lab Chip*, 2007, **7**, 71–76.
- 6 A. Revzin, R. G. Tompkins and M. Toner, *Langmuir*, 2003, **19**, 9855–9862.
- 7 A. Rosenthal, A. Macdonald and J. Voldman, *Biomaterials*, 2007, **28**, 3208–3216.
- 8 A. Folch, B. H. Jo, O. Hurtado, D. J. Beebe and M. Toner, *J. Biomed. Mater. Res.*, 2000, **52**, 346–353.
- 9 M. Ozkan, T. Pisanic, J. Scheel, C. Barlow, S. Esener and S. N. Bhatia, *Langmuir*, 2003, **19**, 1532–1538.
- 10 D. R. Albrecht, G. H. Underhill, T. B. Wassermann, R. L. Sah and S. N. Bhatia, *Nat. Methods*, 2006, **3**, 369–375.
- 11 S. Takayama, J. C. McDonald, E. Ostuni, M. N. Liang, P. J. Kenis, R. F. Ismagilov and G. M. Whitesides, *Proc. Natl. Acad. Sci. U. S. A.*, 1999, **96**, 5545–5548.
- 12 W. Tan and T. A. Desai, *Biomaterials*, 2004, **25**, 1355–1364.
- 13 I. R. Perch-Nielsen, P. J. Rodrigo, C. A. Alonzo and J. Glückstad, *Opt. Express*, 2006, **14**, 12199–12205.
- 14 E. Alsberg, E. Feinstein, M. P. Joy, M. Prentiss and D. E. Ingber, *Tissue Eng.*, 2006, **12**, 3247–3256.
- 15 U. Mirsaidov, W. Timp, K. Timp, M. Mir, P. Matsudaira and G. Timp, *Phys. Rev. E: Stat., Nonlinear, Soft Matter Phys.*, 2008, **78**, DOI: 10.1103/021910.
- 16 K. C. Neuman, E. H. Chadd, G. F. Liou, K. Bergman and S. M. Block, *Biophys. J.*, 1999, **77**, 2856–2863.
- 17 P. Watnick and R. Kolter, *J. Bacteriol.*, 2000, **182**, 2675.
- 18 P. Jordan, H. Clare, L. Flendrig, J. Leach, J. Cooper and M. Padgett, *J. Mod. Opt.*, 2004, **51**, 627–632.
- 19 P. Jordan, J. Leach, M. Padgett, P. Blackburn, N. Isaacs, M. Goksor, D. Hanstorp, A. Wright, J. Girkin and J. Cooper, *Lab Chip*, 2005, **5**, 1224–1228.
- 20 G. M. Cruise, D. S. Scharp and J. A. Hubbell, *Biomaterials*, 1998, **19**, 1287–1294.
- 21 K. T. Nguyen and J. L. West, *Biomaterials*, 2002, **23**, 4307–4314.
- 22 B. C. Kim and M. B. Gu, *Biosens. Bioelectron.*, 2003, **18**, 1015–1021.
- 23 D. Dendukuri, D. C. Pregibon, J. Collins, T. A. Hatton and P. S. Doyle, *Nat. Mater.*, 2006, **5**, 365–369.
- 24 G. Sinclair, P. Jordan, J. Leach, M. J. Padgett and J. Cooper, *J. Mod. Opt.*, 2004, **51**, 409–414.
- 25 M. S. Hahn, J. S. Miller and J. L. West, *Adv. Mater.*, 2006, **18**, 2679–2679.
- 26 G. M. Akselrod, W. Timp, U. Mirsaidov, Q. Zhao, C. Li, R. Timp, K. Timp, P. Matsudaira and G. Timp, *Biophys. J.*, 2006, **91**, 3465–3473.
- 27 J. C. Crocker and D. G. Grier, *J. Colloid Interface Sci.*, 1996, **179**, 298–310.
- 28 A. M. Christensen, D. A. Chang-Yen and B. K. Gale, *J. Micromech. Microeng.*, 2005, **15**, 928–934.
- 29 W. G. Koh, A. Revzin, A. Simonian, T. Reeves and M. Pishko, *Biomed. Microdevices*, 2003, **5**, 11–19.
- 30 G. H. Underhill, A. A. Chen, D. R. Albrecht and S. N. Bhatia, *Biomaterials*, 2007, **28**, 256–270.
- 31 M. A. McClain, C. T. Culbertson, S. C. Jacobson and J. M. Ramsey, *Anal. Chem.*, 2001, **73**, 5334–5338.
- 32 V. A. Soifer, V. Kotlyar and L. Doskolovich, *Iterative methods for diffractive optical elements computation*, Taylor & Francis, London, 1997.
- 33 *Carl Zeiss Objective Transmission Technical Notes*.
- 34 K. Lewis, *Antimicrob. Agents Chemother.*, 2001, **45**, 999.